Journal of Theoretical and Applied Information Technology
10th May 2016. Vol.87. No.1

ISSN: 1992-8645 www.jatit.org E-ISSN: 1817-3195

ADAPTIVE NONLINEAR CONTROL OF DOUBLY-FED INDUCTION MACHINE IN WIND POWER GENERATION

[1]MOHAMMED RACHIDI, [2]BADR BOUOULID IDRISSI
[1,2]Department of Electromechanical Engineering, Moulay Ismaïl University, Ecole Nationale Supérieure d'Arts et Métiers, BP 4024, Marjane II, Beni Hamed, 50000, Meknès, Morocco
E-mail: [1]morachidi@yahoo.fr, [2]badr.bououlid@gmail.com

ABSTRACT

This paper presents an adaptive nonlinear controller for Doubly-Fed Induction Generator (DFIG) in wind power generation. The control objective is to extract the maximum power (Maximum Power Point Tracking) and have a specified reactive power at the generator terminal despite the variable wind speed and the unknown mechanical parameters and mechanical torque. To achieve such a decoupled control, the nonlinear Backstepping approach was combined with the field orientation principle. The induction machine is controlled in a synchronously reference frame oriented along the stator voltage vector position. The mathematical development of the nonlinear Backstepping controller design is examined in detail. The overall stability of the system is shown using Lyapunov approach. Application example on stabilizing a DFIG-based Wind Energy Conversion System (WECS) subject to large mechanical parameters uncertainties has been given to illustrate the design method and confirm the robustness and validity of the proposed control.

Keywords: *Wind Energy Conversion System, Doubly-Fed Induction Generator, Unknown Mechanical Parameters and Torque, Adaptive Nonlinear control, Lyapunov Approach.*

1. INTRODUCTION

Modern wind turbines generators can work at variable wind speed and produce fixed frequency electricity. These variable speed fixed frequency generators use DFIG with a partial converter interface or Permanent Magnet (PM) synchronous generator with a full-converter interface. For high-power wind generation, DFIG-based electric power conversion systems are currently dominating the market. A key DFIG benefit is that inverter rating is typically 25% of total system power which gives a substantial reduction in the power electronics cost as compared with direct-in-line synchronous generator systems. The power percentage fed through the rotor converter is proportional to the slip. At synchronous speed, the only power that flows through the converter is what is needed for ensuring the flow of DC excitation current through rotor windings. Additionally, DFIG systems offer the following advantages:

- The speed range is ±30% around the synchronous speed [1-2]. This allows to continuously operating the wind turbine at its optimum Tip Speed Ratio (TSR), which is specific to the aerodynamic design of a given turbine. This achieves maximum rotor efficiency and hence maximum power extraction.
- Reduced cost of the inverter filters and EMI filters, because filters are rated for 0.25 p.u. total system power.
- Power-factor control can be implemented at lower cost. The four-quadrant converter in the rotor circuit enables decoupled control of active and reactive power of the generator.

However, DFIG-based WECS control is a complex issue [3-8]. Indeed, this system is characterized by multiple variables and operates in environments with extreme variations in the operating conditions (wind speed variation, electrical energy consumption, etc.). On the other hand, DFIG-based drive system is a nonlinear system which is subject to parameter uncertainties and/or time-varying dynamics. The control challenge is to keep the generator at its maximum efficiency despite the wind speed variations and system's parameters uncertainties. In this work, we propose an adaptive nonlinear Backstepping controller design to extract the maximum active power and have a specified reactive power at the generator terminal even in the presence of wind speed variations. The proposed controller also stabilizes the DFIG-based WECS

Journal of Theoretical and Applied Information Technology
10th May 2016. Vol.87. No.1

ISSN: 1992-8645 www.jatit.org E-ISSN: 1817-3195

even in the case of large changes in the damping coefficient and moment of inertia, and mechanical torque. In practice, the damping coefficient and moment of inertia are approximately known and the mechanical torque is a random process variable. To still ensure the stability condition despite parameter change, suitable update laws are derived.

A basic view of the DFIG-based WECS is illustrated in the figure 1. In this system, the power captured by the wind turbine is converted into electrical power by the generator and it is transmitted to the grid by the stator and the rotor windings. The rotor circuit is connected to the grid through a back-to-back converter. The capacitor connected on the DC side acts as the DC voltage source. The electrical grid frequency and voltage magnitude are assumed to be constant.

The control system generates the pitch angle command and the voltage command signals for converters. The grid-side converter (GSC) is controlled to have unity power factor and a constant voltage at the DC-link. The rotor-side converter (RSC) is controlled to have optimal power extraction from the wind and a specified reactive power at the generator terminal.

The paper is structured as follows. The second section presents a state-space modelling of the DFIG-based wind power conversion system. The induction machine is controlled in a rotating reference frame oriented along the stator voltage vector position. The third section describes the proposed nonlinear controller design and gives control and update laws for both RSC and GSC converters. An application example on stabilizing a DIFG-based wind power conversion system subject to large mechanical parameters variations will be given in the last section to show the merits of the proposed controller. Simulation results and analysis confirm the effectiveness of the proposed approach.

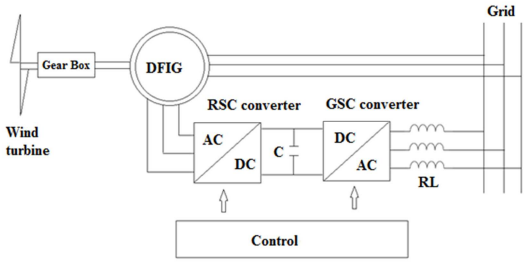

Figure. 1: DFIG-based wind power conversion system

2. SYSTEM MODEL

2.1. Modelling of the Wind Turbine

The aerodynamic turbine power P_t depends on the power coefficient C_p as follows [9]:

$$P_t = \frac{1}{2}\rho\,\pi\,R_t^2\,C_p(\lambda,\beta)\,v^3 \quad (1a)$$

where:

- ρ: Specific mass of the air (kg/m^2);
- v: Wind speed (m/s);
- R_t: Radius of turbine (m);
- C_p: Power coefficient;
- β: Blade pitch angle (deg);
- Ω: Generator speed (rad/s);
- λ: Tip Speed Ratio (TSR) of the rotor blade tip speed to wind speed.

The TSR is given by:

$$\lambda = \frac{R_t\,\Omega}{G\,v} \quad (1b)$$

where G is mechanical speed multiplier. A generic equation is used to model $c_p(\lambda,\beta)$, based on the modeling turbine characteristics of [9]:

$$C_p(\lambda,\beta) = c_1\left(\frac{c_2}{\lambda_i} - c_3\beta - c_4\right)\exp\left(-\frac{c_5}{\lambda_i}\right) + c_6\lambda \quad (1c)$$

Where $\frac{1}{\lambda_i} = \frac{1}{\lambda + 0.08\beta} - \frac{0.035}{\beta^3 + 1}$

and the coefficients c_1 to c_6 are: $c_1 = 0.5176$, $c_2 = 116$, $c_3 = 0.4$, $c_4 = 5$, $c_5 = 21$ and $c_6 = 0.0068$.

Note that the maximum value of c_p (c_{pmax}= 0.48) is achieved for $\beta = 0°$ and $\lambda = \lambda_{opt}$ =8.1.
In this work, we assume that the wind turbine operates with β=0. To capture the maximum power, a speed controller must control the mechanical speed Ω so as to track a speed reference Ω_c that keeps the system at λ_{opt} (Maximum Power Point Tracking strategy). According to (1b), the optimal mechanical speed is:

$$\Omega_c = \frac{G\,v}{R_t\,\lambda_{opt}} \quad (1d)$$

2.2. Induction Generator Model

The induction machine is controlled in a synchronously rotating dq axis frame, with the d-axis oriented along the stator-voltage vector position (v_{sd}=V, v_{sq}=0). In this reference frame, the electromechanical equations are [10]:

$$[V] = [R][I] + \frac{d[\phi]}{dt} + [\omega][\phi] \quad (2a)$$

$$[\phi] = [M][I] \quad (2b)$$

Journal of Theoretical and Applied Information Technology
10th May 2016. Vol.87. No.1

ISSN: 1992-8645 www.jatit.org E-ISSN: 1817-3195

$$J\frac{d\Omega}{dt} = T_t - T_{em} - F\Omega \quad (2c)$$

$$T_{em} = pL_m(i_{sq}i_{rd} - i_{sd}i_{rq}) \quad (2d)$$

where:

$$[R]=\begin{bmatrix} Rs & 0 & 0 & 0 \\ 0 & Rs & 0 & 0 \\ 0 & 0 & Rr & 0 \\ 0 & 0 & 0 & Rr \end{bmatrix}; [M]=\begin{bmatrix} Ls & 0 & L_m & 0 \\ 0 & Ls & 0 & L_m \\ L_m & 0 & Lr & 0 \\ 0 & L_m & 0 & Lr \end{bmatrix};$$

$$[\omega]=\begin{bmatrix} 0 & -\omega_s & 0 & 0 \\ \omega_s & 0 & 0 & 0 \\ 0 & 0 & 0 & -\omega_r \\ 0 & 0 & \omega_r & 0 \end{bmatrix}$$

[V], [I] and [φ] are respectively voltage, current and flux vectors.

The subscripts s, r, d and q stand respectively for stator, rotor, direct and quadratic.

R, L, L_m, ω, J, F, p, T_t and T_{em} denote respectively resistance, inductance, mutual inductance, electrical speed, total inertia, damping coefficient, number of pole pairs, mechanical torque and electromagnetic torque.

By selecting currents and speed as the state variables, the system (2) can be put into the following state-space form:

$$\dot{x}_1 = g_1(x) - \beta u_1 \quad (3a)$$

$$\dot{x}_2 = g_2(x) - \beta u_2 \quad (3b)$$

$$\dot{x}_3 = g_3(x) + \alpha u_1 \quad (3c)$$

$$\dot{x}_4 = g_4(x) + \alpha u_2 \quad (3d)$$

$$\dot{\eta} = \frac{1}{J}(-F\eta + T_t - T_{em}) = \frac{1}{J}(-F\eta + T_t - h(x)) \quad (3e)$$

Where

$$x = (x_1, x_2, x_3, x_4)^t = (i_{sd}, i_{sq}, i_{rd}, i_{rq})^t, \eta = \Omega$$

$$h(x) = T_{em} = a(x_2x_3 - x_1x_4)$$

$$u_1 = v_{rd}, u_2 = v_{rq}$$

$$\alpha = \frac{1}{\sigma L_r}, \beta = \frac{L_m}{\sigma L_r L_s}$$

$$g_1(x) = -a_1x_1 + b_1x_2 + c_1x_3 + m_1x_2\eta + n_1x_4\eta + \alpha_u$$
$$g_2(x) = -b_1x_1 - a_1x_2 + c_1x_4 - m_1x_1\eta - n_1x_3\eta$$
$$g_3(x) = c_3x_1 - a_3x_3 + b_3x_4 - n_3x_2\eta - m_3x_4\eta - \beta_u$$
$$g_4(x) = c_3x_2 - b_3x_3 - a_3x_4 + n_3x_1\eta + m_3x_3\eta$$

$$a = pL_m,\ a_1 = \frac{R_s}{\sigma L_s}, b_1 = \omega_s = 2\pi f, c_1 = \frac{L_m R_r}{\sigma L_s L_r},$$

$$m_1 = p\frac{1-\sigma}{\sigma}, n_1 = p\frac{L_m}{\sigma L_s}, \alpha_u = \frac{1}{\sigma L_s}V, a_3 = \frac{R_r}{\sigma L_r},$$

$$b_3 = 2\pi f, c_3 = \frac{L_m R_s}{\sigma L_s L_r}, m_3 = \frac{p}{\sigma}, n_3 = p\frac{L_m}{\sigma L_r},$$

$$\beta_u = \beta V; \sigma = 1 - \frac{L_m^2}{L_s L_r}$$

f and V are respectively the constant frequency and magnitude of grid voltage.

Equations (3a) to (3.d) can be put into the following compact form:

$$\dot{x} = g(x) + Au \quad (3f)$$

where

$$g(x) = (g_1(x), g_2(x), g_3(x), g_4(x))^t,\ u = (u_1, u_2)^t,$$
$$A = \begin{bmatrix} -\beta & 0 & \alpha & 0 \\ 0 & -\beta & 0 & \alpha \end{bmatrix}$$

2.3. DC-link and Coupling Filter R-L Models

The GSC converter is connected to the grid through an R-L filter (fig 2) [11].

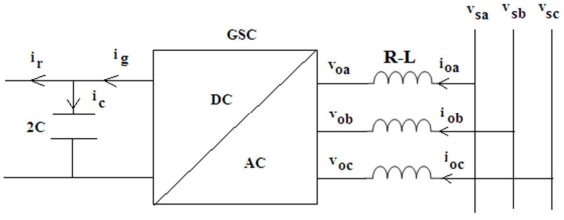

Figure.2: DC-link and RL filter sign conventions

By using Kirchhoff's laws and Park transformation, we obtain the R-L filter dynamic equations in the synchronous reference frame:

$$\begin{cases} v_{sd} = Ri_{0d} + L\frac{di_{0d}}{dt} - \omega_s i_{0q} + v_{0d} = V \\ v_{sq} = Ri_{0q} + L\frac{di_{0q}}{dt} + \omega_s i_{0d} + v_{0q} = 0 \end{cases} \quad (4a)$$

Journal of Theoretical and Applied Information Technology
10th May 2016. Vol.87. No.1

ISSN: 1992-8645 www.jatit.org E-ISSN: 1817-3195

Neglecting losses, the DC-link dynamic equations are:

$$\begin{cases} 2C\dfrac{dV_{dc}}{dt} = i_g - i_r \\ v_{sd}i_{0d} + v_{sq}i_{0q} = V_{dc}i_g \\ u_1x_3 + u_2x_4 = V_{dc}i_r \end{cases} \quad (4b)$$

Equations (4a) and (4b) can be put into the following state-space form:

$$\dot{\zeta}_1 = -b\zeta_1 + c\zeta_2 - \mu + \lambda v_1 = f_1(\zeta) + \lambda v_1 \quad (4c)$$

$$\dot{\zeta}_2 = -c\zeta_1 - b\zeta_2 + \lambda v_2 = f_2(\zeta) + \lambda v_2 \quad (4d)$$

$$\dot{\zeta}_3 = \alpha(x,u) + \gamma\zeta_1 \quad (4e)$$

where

$$\zeta_1 = i_{od};\ \zeta_2 = i_{oq};\ \zeta_3 = V_{dc}^2;\ v_1 = v_{od};\ v_2 = v_{oq};$$

$$b = \frac{R}{L},\quad c = \frac{\omega_s}{L},\quad \mu = -\frac{V}{L},\quad \lambda = -\frac{1}{L}$$

$$\alpha(x,u) = -\frac{1}{C}(u_1x_3 + u_2x_4),\quad \gamma = \frac{V}{C}$$

3. CONTROL DESIGN

3.1. RSC Control

3.1.1. Backstepping control strategy

The RSC converter enables decoupled control of stator reactive power and speed. Indeed, the following expression of the stator reactive power

$$Q_{sg} = \mathrm{Im}(\underline{V}\,\underline{I}^*) = v_{sq}i_{sd} - v_{sd}i_{sq} = -V x_2 \quad (5a)$$

shows that the current variable x_2 can be considered as a virtual control of Q_{sg}. According to equation (3b), it is clear that the control variable u_2 can be designed so that the current variable x_2 tracks its reference. On the other hand, equation (3e) shows that the electromagnetic torque T_{em} can be considered as a virtual control for the speed η. The following dynamic equation

$$\begin{aligned} \dot{T}_{em} &= \upsilon \\ &= \nabla h\,.g + a\,(\alpha x_2 + \beta x_4)\,u_1 - a\,(\alpha x_1 + \beta x_3)\,u_2 \end{aligned} \quad (5b)$$

shows that the control variable u_1 can be designed so that the electromagnetic torque T_{em} tracks its reference.

3.1.2. Control and update laws

In the case of uncertain model where system parameters are not known with enough accuracy, suitable choice of control variables and update laws must be done to still ensure the stability condition [11-14]. In this study, it is assumed that the mechanical parameters F, J and mechanical torque T_t are unknown. F and J are constant parameters whilst the torque T_t is assumed to vary slowly in time. Estimates of F, J and T_t are denoted $\hat{F}$, $\hat{J}$ and $\hat{T}_t$, respectively. η_c, T_{emc} and x_{2c} are references of the variables η, T_{em} and x_2, respectively.

We define the following error variables:

$$z_0 = x_2 - x_{2c}$$
$$z_1 = \eta - \eta_c$$
$$z_2 = T_{em} - T_{emc}$$
$$\tilde{J} = J - \hat{J}$$
$$\tilde{F} = F - \hat{F}$$
$$\tilde{T}_t = T_t - \hat{T}_t$$
$$\tilde{\theta} = \theta - \hat{\theta} \quad \text{with } \theta = (F, J, T_t)^t,\ \tilde{\theta} = (\tilde{F}, \tilde{J}, \tilde{T}_t)^t,$$
$$\hat{\theta} = (\hat{F}, \hat{J}, \hat{T}_t)^t$$

Proposition 1: The following control and update laws:

$$u_1 = \frac{\upsilon - (k_2 + k_1)z_2 + a u_2(\beta x_3 + \alpha x_1)}{a(\alpha x_2 + \beta x_4)}$$

$$u_2 = \frac{k_0 z_0 + g_2(x) - \dot{x}_{2c}}{\beta}$$

$$\dot{\hat{F}} = \gamma_1(z_2^2 - \eta z_1 + \eta z_2 \varphi(\hat{\theta}))$$

$$\dot{\hat{T}}_t = \gamma_2(z_1 - z_2\varphi(\hat{\theta}))$$

$$\dot{\hat{J}} = -\gamma_3(k_1 z_2^2 + (\dot{\eta}_c - k_1 z_1)(z_1 - z_2\varphi(\hat{\theta})))$$

with

$$\upsilon = \nabla\psi.\dot{\xi} - k_1 z_1 \varphi(\hat{\theta}) - \nabla h.g$$

$$\psi(\xi, z_1) = T_{emc} = -\hat{J}(\dot{\eta}_c - k_1 z_1) + \hat{T}_t - (z_1 + \eta_c)\hat{F}$$

$$\xi = (\eta_c, \dot{\eta}_c, \hat{J}, \hat{F}, \hat{T}_t)$$

$$\varphi(\hat{\theta}) = k_1\hat{J} - \hat{F}$$

$k_0, k_1, k_2, \gamma_1, \gamma_2$ and γ_3 are *positives design constants*

achieve speed and current tracking objectives and ensure asymptotic stability despite the changes in mechanical parameters.

ISSN: 1992-8645 www.jatit.org E-ISSN: 1817-3195

Proof:

a- Control law u_2

Taking the derivative of z_0 and using (3b) gives:

$$\dot{z}_0 = g_2(x) - \beta u_2 - \dot{x}_{2c} \quad (6)$$

Let $V_0 = \frac{1}{2} z_0^2$ be the Lyapunov candidate function; the choice $\dot{z}_0 = -k_0 z_0$, where k_0 is a positive design constant, makes negative the derivative $\dot{V}_0 = z_0 \dot{z}_0$ since $\dot{V}_0 = -k_0 z_0^2 \le 0$. With this choice, the control law u_2 can be obtained from equation (6):

$$u_2 = \frac{g_2(x) + k_0 z_0 - \dot{x}_{2c}}{\beta} \quad (7)$$

b- Control u_1 and update laws

Step 1: Virtual control T_{emc}

Using equation (3e), the derivative of z_1 is written as:

$$\dot{z}_1 = \frac{-F\eta + T_t - T_{em}}{J} - \dot{\eta}_c \quad (8)$$

Since J, F and T_t are unknown; it will be replaced with their estimates $\hat{F}, \hat{J}$ and $\hat{T}_t$, respectively. Let $V_1 = \frac{1}{2} z_1^2$ be the Lyapunov candidate function; the choice $\dot{z}_1 = -k_1 z_1$, where k_1 is a positive design constant, makes negative the derivative $\dot{V}_1 = z_1 \dot{z}_1$ since $\dot{V}_1 = -k_1 z_1^2 \le 0$.

Thus, equation (8) gives:

$$-k_1 z_1 = \frac{-\hat{F}\eta + \hat{T}_t - T_{emc}}{\hat{J}} - \dot{\eta}_c \quad (9)$$

which yields the following expression of the virtual control T_{emc}:

$$\begin{aligned} T_{emc} &= -\hat{J}(\dot{\eta}_C - k_1 z_1) + \hat{T}_t - \hat{F}(z_1 + \eta_c) \\ &= \psi(\xi, z_1) \end{aligned} \quad (10)$$

where η has been replaced by $z_1 + \eta_c$ and $\xi = (\eta_c, \dot{\eta}_C, \hat{J}, \hat{F}, \hat{T}_t)$.

Step 2: Control u_1 and update laws

Equation (8) can be written as:

$$\dot{z}_1 = \frac{-\tilde{F}\eta + \tilde{T}_t - z_2}{J} + \frac{-\hat{F}\eta + \hat{T}_t - T_{emc}}{J} - \dot{\eta}_c \quad (11)$$

Subtracting (9) from (11) yields:

$$\dot{z}_1 = -k_1 z_1 - \frac{z_2}{J} + \tilde{A} \quad (12)$$

where $\tilde{A} = \frac{\tilde{T}_t}{J} - \eta \frac{\tilde{F}}{J} + (k_1 z_1 - \dot{\eta}_C) \frac{\tilde{J}}{J}$.

On the other hand, the derivative of z_2 is:

$$\dot{z}_2 = \upsilon - \dot{T}_{emc}$$

Using (10) and (12):

$$\begin{aligned} \dot{T}_{emc} &= \nabla\psi . \dot{\xi} + \frac{\partial \psi}{\partial z_1} \dot{z}_1 \\ &= \nabla\psi . \dot{\xi} - k_1 z_1 \varphi(\hat{\theta}) - \frac{\varphi(\hat{\theta})}{J} z_2 + \varphi(\hat{\theta}) \tilde{A} \end{aligned}$$

where $\varphi(\hat{\theta}) = \frac{\partial \psi}{\partial z_1} = k_1 \hat{J} - \hat{F}$.

Since:

$$\begin{aligned} \frac{\varphi(\hat{\theta})}{J} &= -\frac{\varphi(\tilde{\theta})}{J} + \frac{\varphi(\theta)}{J} \\ &= -\frac{\varphi(\tilde{\theta})}{J} + k_1 - \frac{F}{J} \end{aligned}$$

The derivative $\dot{z}_2$ becomes:

$$\begin{aligned} \dot{z}_2 &= \upsilon - \nabla\psi . \dot{\xi} + k_1 z_1 \varphi(\hat{\theta}) - \varphi(\tilde{\theta}) \frac{z_2}{J} - \frac{F}{J} z_2 \\ &\quad + k_1 z_2 - \varphi(\hat{\theta}) \tilde{A} \\ &= B - \frac{F}{J} z_2 + \tilde{C} \end{aligned} \quad (13)$$

with

$$B = \upsilon - \nabla\psi . \dot{\xi} + k_1 z_1 \varphi(\hat{\theta}) + k_1 z_2$$

$$\tilde{C} = -\varphi(\tilde{\theta}) \frac{z_2}{J} - \varphi(\hat{\theta}) \tilde{A}$$

To design the control u_1 and update laws, we consider the following Lyapunov candidate function:

$$V_1 = \frac{1}{2} z_1^2 + \frac{1}{2} z_2^2 + \frac{1}{2\gamma_1} \frac{\tilde{F}^2}{J} + \frac{1}{2\gamma_2} \frac{\tilde{T}_t^2}{J} + \frac{1}{2\gamma_3} \frac{\tilde{J}^2}{J}$$

Its derivative is given by:

ISSN: 1992-8645 www.jatit.org E-ISSN: 1817-3195

$$\dot{V}_1 = z_1\dot{z}_1 + z_2\dot{z}_2 - \frac{1}{\gamma_1}\frac{\tilde{F}}{J}\dot{\hat{F}} - \frac{1}{\gamma_2}\frac{\tilde{T}_t}{J}\dot{\hat{T}}_t - \frac{1}{\gamma_3}\frac{\tilde{J}}{J}\dot{\hat{J}}$$

Using (12) and (13), $\dot{V}_1$ can be written as follows:

$$\dot{V}_1 = -k_1 z_1^{\,2} - \frac{z_1 z_2}{J} - \frac{F}{J}z_2^2 + z_2 B + \tilde{D}$$

with

$$\begin{aligned}\tilde{D} &= z_1\tilde{A} + z_2\tilde{C} - \frac{1}{\gamma_1}\frac{\tilde{F}}{J}\dot{\hat{F}} - \frac{1}{\gamma_2}\frac{\tilde{T}_t}{J}\dot{\hat{T}}_t - \frac{1}{\gamma_3}\frac{\tilde{J}}{J}\dot{\hat{J}} \\ &= \left[z_2^2 - \eta(z_1 - z_2\varphi(\hat{\theta})) - \frac{\dot{\hat{F}}}{\gamma_1}\right]\frac{\tilde{F}}{J} \\ &\quad + \left[z_1 - z_2\varphi(\hat{\theta}) - \frac{\dot{\hat{T}}_t}{\gamma_2}\right]\frac{\tilde{T}_t}{J} \\ &\quad + \left[-k_1 z_2^2 + (z_1 - z_2\varphi(\hat{\theta}))(k_1 z_1 - \dot{\eta}_C) - \frac{\dot{\hat{J}}}{\gamma_3}\right]\frac{\tilde{J}}{J}\end{aligned}$$

The update laws are obtained by cancelling the terms with $\frac{\tilde{J}}{J}, \frac{\tilde{F}}{J}$ and $\frac{\tilde{T}_t}{J}$:

$$\begin{aligned}\dot{\hat{F}} &= \gamma_1(z_2^2 - \eta z_1 + \eta z_2\varphi(\hat{\theta})) \\ \dot{\hat{T}}_t &= \gamma_2(z_1 - z_2\varphi(\hat{\theta})) \\ \dot{\hat{J}} &= -\gamma_3(k_1 z_2^2 + (\dot{\eta}_c - k_1 z_1)(z_1 - z_2\varphi(\hat{\theta}))\end{aligned} \qquad (14)$$

Subsequently, the derivative $\dot{V}_1$ reduces to:

$$\dot{V}_1 = -k_1 z_1^{\,2} - \frac{z_1 z_2}{J} - \frac{F}{J}z_2^2 + z_2 B$$

We choose $B = -k_2 z_2$, with k_2 is a positive design constant. Since $-z_1 z_2 \le \frac{z_1^2 + z_2^2}{2}$ for all z_1, z_2, we have:

$$\begin{aligned}\dot{V}_1 &= -k_1 z_1^{\,2} - \frac{z_1 z_2}{J} - \frac{F}{J}z_2^2 - k_2 z_2^2 \\ &\le -(k_1 - \frac{1}{2J})z_1^2 - (k_2 + \frac{F}{J} - \frac{1}{2J})z_2^2\end{aligned}$$

By selecting k_1 and k_2 such that the inequalities $k_1 > \frac{1}{2J}$ and $k_2 > \frac{1}{2J}$ are verified, the derivative $\dot{V}_1$ becomes negative and so we ensure the stability condition.

The control variable υ can then be obtained using equation (13) and the choice $B = -k_2 z_2$:

$$\upsilon = \nabla\psi.\dot{\xi} - k_1 z_1\varphi(\hat{\theta}) - (k_1 + k_2)z_2$$

Finally, equation (5b) gives the control law u_1:

$$u_1 = \frac{\upsilon - (k_2 + k_1)z_2 + a u_2(\beta x_3 + \alpha x_1)}{a(\alpha x_2 + \beta x_4)} \qquad (15)$$

Where

$$\begin{aligned}\nabla\psi.\dot{\xi} &= \frac{\partial\psi}{\partial\eta_c}\dot{\eta}_c + \frac{\partial\psi}{\partial\dot{\eta}_C}\ddot{\eta}_c + \frac{\partial\psi}{\partial\hat{J}}\dot{\hat{J}} + \frac{\partial\psi}{\partial\hat{F}}\dot{\hat{F}} + \frac{\partial\psi}{\partial\hat{T}_t}\dot{\hat{T}}_t \\ &= -\hat{F}\dot{\eta}_c - \hat{J}\ddot{\eta}_c - (\dot{\eta}_c - k_1 z_1)\dot{\hat{J}} - (z_1 + \eta_c)\dot{\hat{F}} + \dot{\hat{T}}\end{aligned}$$

and

$$\nabla h.g = a(x_2 g_3(x) + x_3 g_2(x) - x_1 g_4(x) - x_4 g_1(x))$$

Remark:

The term $a(\alpha x_2 + \beta x_4)$ is proportional to q-axis flux ϕ_{sq}:

$$\begin{aligned}a(\alpha x_2 + \beta x_4) &= a(\frac{1}{\sigma L_r}i_{sq} + \frac{L_m}{\sigma L_s L_r}i_{rq}) \\ &= \frac{a}{\sigma L_s L_r}(L_s i_{sq} + L_m i_{rq}) \\ &= \frac{a}{\sigma L_s L_r}\phi_{sq}\end{aligned}$$

Since the effect of the stator resistance is negligible especially in high power, and the stator voltage vector is aligned along the d-axis of the reference frame, the amplitude $|\phi_{sq}|$ is proportional to voltage V. Hence, the term $|a(\alpha x_2 + \beta x_4)|$ becomes different from zero as soon as the machine is connected to the grid.

3.2. GSC Control

3.2.1. Backstepping control strategy

The GSC converter enables decoupled control of rotor reactive power and DC-link voltage. Indeed, the following expression of the rotor reactive power

$$Q_{rg} = \mathrm{Im}(\underline{V}\,\underline{I}^*) = v_{sq} i_{od} - v_{sd} i_{oq} = -V\zeta_2 \qquad (16)$$

shows that the current variable ζ_2 can be considered as a virtual control of Q_{rg}. According to equation (4d), it is clear that the control variable v_2

ISSN: 1992-8645 www.jatit.org E-ISSN: 1817-3195

can be designed so that the current variable ζ_2 tracks its reference. On the other hand, equation (4e) shows that ζ_1 can be considered as a virtual control for DC-link voltage. Equation (4c) shows that the control variable v_1 can be designed so that ζ_1 tracks its reference.

3.2.2. Control laws

We define the following error variables:

$$e_1 = \zeta_1 - \zeta_{1c} \quad (16a)$$
$$e_2 = \zeta_2 - \zeta_{2c} \quad (16b)$$
$$e_3 = \zeta_3 - \zeta_{3c} \quad (16c)$$

where ζ_{1c}, ζ_{2c} and ζ_{3c} are references of ζ_1, ζ_2 and ζ_3, respectively.

Proposition 2: *The following control laws:*

$$v_1 = \frac{\ddot{\zeta}_{3c} + (q_3^2 - \gamma^2)e_3 - (q_3 + q_1)\gamma e_1 - \dot{\alpha}(x,u) - \gamma f_1(\zeta)}{\gamma\lambda}$$

$$v_2 = \frac{-q_2 e_2 - f_2(\zeta) + \dot{\zeta}_{2c}}{\lambda}$$

With q_1, q_2 and q_3 are positive design constants,

achieve the DC-link voltage and rotor reactive power control objective and ensure the asymptotic stability.

Proof:

a- Control law v_2

According to (4d), the dynamic equation of the error e_2 is:

$$\dot{e}_2 = f_2(\zeta) + \lambda v_2 - \dot{\zeta}_{2c} \quad (17)$$

To reduce the tracking error, we use the following Lyapunov candidate function $V_2 = \frac{1}{2}e_2^2$. The choice $\dot{e}_2 = -q_2 e_2$, where q_2 is a positive design constant, makes negative the derivative $\dot{V}_2 = e_2\dot{e}_2$ since $\dot{V}_2 = -q_2 e_2^2 \le 0$. With this choice, the control law v_2 can be obtained from equation (17):

$$v_2 = \frac{-q_2 e_2 - f_2(\zeta) + \dot{\zeta}_{2c}}{\lambda} \quad (18)$$

b- Control law v_1

Step 1: Virtual control ζ_{1c}

According to (4e), the dynamic equation of the error e_3 is:

$$\dot{e}_3 = \alpha(x,u) + \gamma\zeta_1 - \dot{\zeta}_{3c} \quad (19)$$

We consider the Lyapunov candidate function $V_3 = \frac{1}{2}e_3^2$. The choice $\dot{e}_3 = -q_3 e_3$, where q_3 is a positive design constant, makes negative the derivative $\dot{V}_3 = e_3\dot{e}_3$ and hence reduces the tracking error e_3. With this choice, the virtual control law ζ_{1c} can be obtained from equation (19):

$$\zeta_{1c} = \frac{-\alpha(x,u) - q_3 e_3 + \dot{\zeta}_{3c}}{\gamma} \quad (20)$$

Step 2: control law v_1

According to (4c), the dynamic equation of the error e_1 is:

$$\dot{e}_1 = f_1(\zeta) + \lambda v_1 - \dot{\zeta}_{1c} \quad (21)$$

The derivative of e_3 can be re-written as:

$$\begin{aligned}\dot{e}_3 &= \alpha(x,u) + \gamma(\zeta_1 - \zeta_{1c}) + \gamma\zeta_{1c} - \dot{\zeta}_{3c} \\ &= \gamma e_1 - q_3 e_3\end{aligned} \quad (22)$$

From (20) and (22), we obtain the derivative $\dot{\zeta}_{1c}$:

$$\dot{\zeta}_{1c} = \frac{-\dot{\alpha}(x,u) - q_3(\gamma e_1 - q_3 e_3) + \ddot{\zeta}_{3c}}{\gamma} \quad (23)$$

We now consider the Lyapunov candidate function:

$$V_g = \frac{1}{2}e_1^2 + \frac{1}{2}e_3^2$$

Its derivative is:

$$\begin{aligned}\dot{V}_g &= e_1\dot{e}_1 + e_3\dot{e}_3 \\ &= e_1\dot{e}_1 + e_3(-q_3 e_3 + \gamma e_1) \\ &= -q_3 e_3^2 + e_1(\dot{e}_1 + \gamma e_3)\end{aligned}$$

With the choice $\dot{e}_1 + \gamma e_3 = -q_1 e_1$, we ensure the negativity of $\dot{V}_g$ since $\dot{V}_g = -q_1 e_1^2 - q_3 e_3^2 \le 0$. Also, equation (21) yields:

$$f_1(\zeta) + \lambda v_1 - \dot{\zeta}_{1c} + \gamma e_3 = -q_1 e_1 \quad (24)$$

From (23) and (24), we obtain the control law v_1:

$$v_1 = \frac{\ddot{\zeta}_{3c} + (q_3^2 - \gamma^2)e_3 - (q_3 + q_1)\gamma e_1 - \dot{\alpha}(x,u) - \gamma f_1(\zeta)}{\gamma\lambda}$$

ISSN: 1992-8645 www.jatit.org E-ISSN: 1817-3195

4. SIMULATION RESULTS

To demonstrate the effectiveness of the proposed controller, two SIMULINK models were constructed which correspond respectively to the conventional (without adaptation) and adaptive (unknown mechanical parameters) Backstepping controllers. The tracking capability was verified for the adaptive controller in the case of time-varying wind speed (Fig. 3). To show the robustness against mechanical parameters and mechanical torque change speed regulation performances were compared at constant wind speed (Fig. 4). Constant values for DC-link voltage, filter and stator quadratic currents references were considered. Design parameters used in the simulation are listed in Table 1.

Table1: Design Parameters

Parameter	Value
k_0	1000
k_1	150
k_2	2000
$\gamma_1, \gamma_2, \gamma_3$	0.0001
q_1, q_2, q_3	100

Figures 3a and 3b confirm the effectiveness of the MPPT strategy since the rotor speed vary in accordance with wind speed so that the turbine operates at optimal TSR.

To have a unity power factor, the references of q-axis currents i_{sq} and i_{oq} have been set to zero. Figures 3c and 3d show the good tracking capability of the q-axis current controller. The same good performance is achieved in the case of DC-link regulation (Figure 3e) and torque controller (Figure 3f).

Figures 3g to 3j illustrate the two operating modes of the generator. At time t=70s, we can see in figure 3b that the induction machine operates at sub-synchronous mode (N<1500 rpm). Figure 3i shows that grid voltage and stator current are in phase, thus the active power is transmitted from the stator to the grid. Figure 3g shows that grid voltage and filter current are in phase opposition, thus the active power is transmitted from the grid to the rotor. This result is compatible with the sub-synchronous speed operation.

At time t=170s, we can see in figure 3b that the induction machine operates at super-synchronous mode (N>1500 rpm). Figure 3j shows that grid voltage and stator current are in phase, thus the active power is transmitted from the stator to grid. Figure (3h) shows that the grid voltage and filter current are in phase, thus the active power is transmitted from the grid to rotor. This result is compatible with the super-synchronous speed operation.

Figure 4 shows speed regulation performance for both conventional and adaptive controllers in the case of change in the coefficients F, J and the mechanical torque T_t. The simulation assumes that changes occur first in the system model (at 100s, ΔF=200%, ΔJ=-50%), and next in the mechanical torque (at 150s, ΔT_t=300%). Unlike the conventional backstepping controller (fig.4.b), the adaptive controller tracks the constant speed reference despite the changes (Fig. 4a). This confirms the robustness of the proposed controller.

5. CONCLUSION

A stable and robust Backstepping controller has been successfully applied to a DFIG-based WECS to extract the maximum power and have a unity power factor despite the wind speed variation and system parameter uncertainties. Simulation results showed the effectiveness of the proposed controller and its superiority over conventional controller. Good speed and current tracking performances were achieved even in the case of large change in the mechanical torque.

Appendix: Characteristics and Parameters

Induction Generator	
Rated power	3MW
Rated stator voltage	690V
Nominal frequency	50Hz
Number of pole pairs	p =2
Rotor resistance	R_s=2.97e-3Ω
Stator resistance	R_r=3.82e-3Ω
Stator inductance	L_s=0.0122H
Rotor inductance	L_r=0.0122H
Mutual inductance	L_m=12.12e-3H
Wind Turbine	
Blade Radius	R_t=45m
Power coefficient	C_{pmax}= 0.48
Optimal TSR	λ_{opt}=8.14
Mechanical speed multiplier	G=100
Generator and Turbine	
Moment of inertia	J=254Kg .m^2
Damping coefficient	F=0.24

ISSN: 1992-8645 www.jatit.org E-ISSN: 1817-3195

Bus DC	C = 38 mF, v_{dc} = 1200 V
Filter RL	R = 0,075 Ω, L = 0,75 mH
Electrical grid	U = 690 V, f = 50 Hz

REFERENCES:

[1] H. Li, Z. Chen, "Overview of different wind generator systems and their comparisons" IET Renewable Power Generation, 2008, 2(2):123-138.

[2] B. Multon ; X. Roboam ; B Dakyo ; C. Nichita ; O Gergaud ; H. Ben Ahmed, "Aérogénérateurs électriques", techniques de l'Ingénieur, Traités de génie électrique, D3960, Novembre 2004.

[3] E. Koutroulis and K. Kalaitzakis, "Design of a Maximum Power Tracking System for Wind-Energy-Conversion Applications" IEEE Transactions On Industrial Electronics, Vol. 53, No. 2, April 2006.

[4] L. L. Freris, "Wind Energy Conversion Systems" Englewood Cliffs, NJ: Prentice-Hall, 1990, pp. 182–184.

[5] Y.Hong, S. Lu, C. Chiou, "MPPT for PM wind generator using gradient approximation", Energy Conversion and Management 50 (1), pp. 82-89, 2009

[6] R. Pena, J. C. Clare, G. M. Asher, "Doubly fed induction generator using back-to-back PWM converters and its application to variable - speed wind-energy generation," IEE Proc. Electr. Power Appl., vol. 143, no. 3, pp. 231-241, May 996.

[7] Peresada, S., A. Tilli and A. Tonielli, "Robust Active-reactive power control of a doubly-fed induction generator". In Proc. IEEE-IECON'1998, Aachen, Germany, pp: 1621-1625.

[8] Karthikeyan A., Kummara S.K, Nagamani C. and Saravana Ilango G, " Power control of grid connected Doubly Fed Induction Generator using Adaptive Back Stepping approach", in Proc 10th IEEE International Conference on Environment and Electrical Engineering EEEIC-2011, Rome, May 2011.

[9] Siegfried Heier, "Grid Integration of Wind Energy Conversion Systems" John Wiley & Sons Ltd, 1998, ISBN 0-471-97143-X

[10] J.P.Caron, J.P.Hautier, 1995 "Modélisation et Commande de la Machine Asynchrone" Edition Technip, Paris.

[11] A.El Magri, F.Giri, A. Elfadili, L. Dugard, "Adaptive Nonlinear Control of Wind Energy Conversion System with PMS Generator" 11th IFAC International Workshop on Adaptation and Learning in Control and Signal Processing, Jul 2013, Caen, France. pp.n/c, 2013.

[12] M. Krstic, I. Kanellakopoulos, P. Kokotovic," Nonlinear and adaptive control design" John Wilay & Sons, Inc, 1995.

[13] I. Kanellakopoulos, P.V. Kokotovic, and A.S. Morse, "Systematic design of adaptive controller for feedback linearizable systems", IEEE Trans. Auto. Control. 1991. Vol. 36, (11), pp. 1241-1253.

[14] H. Tan, J. Chang, "Field orientation and adaptive backstepping for induction motor control" IEEE Proc. 1999.

Journal of Theoretical and Applied Information Technology
10th May 2016. Vol.87. No.1

ISSN: 1992-8645 www.jatit.org E-ISSN: 1817-3195

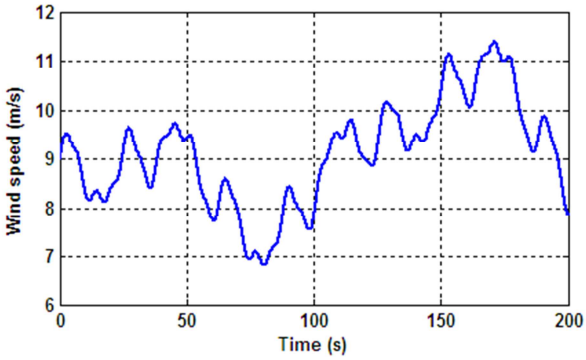

Figure. 3a: Time-varying wind speed

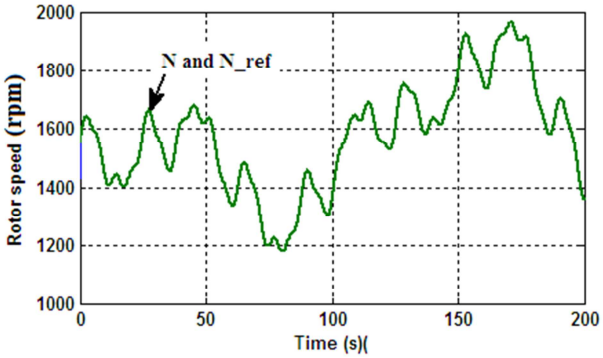

Figure. 3b: Rotor speed and its reference

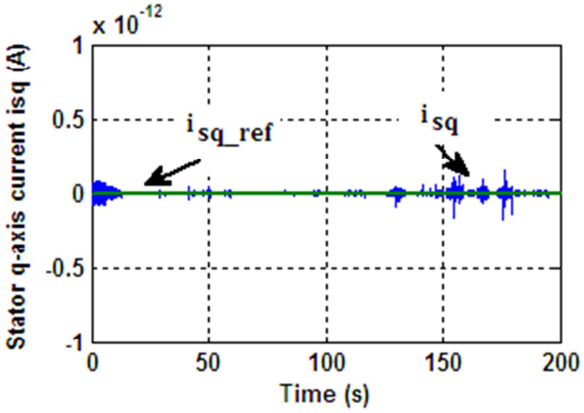

Figure. 3c: Stator q-axis current and its reference

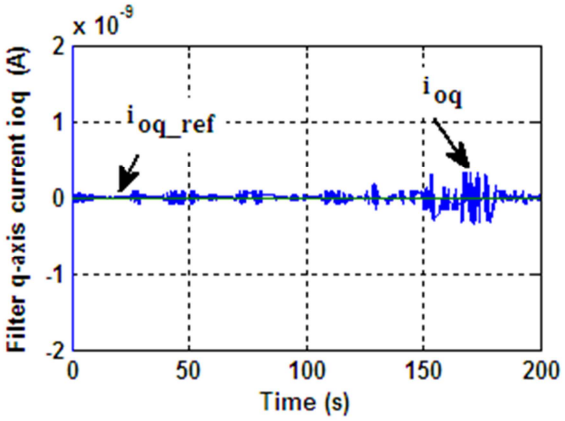

Figure. 3d: Filter q-axis current and its reference

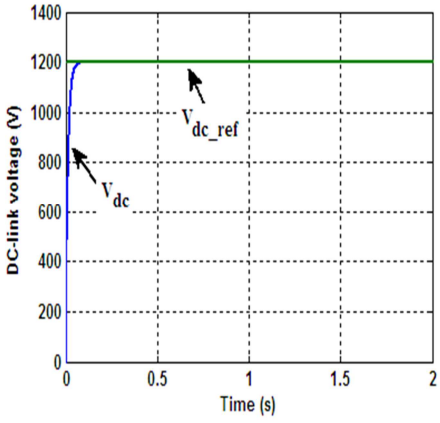

Figure. 3e: DC-link voltage and its reference

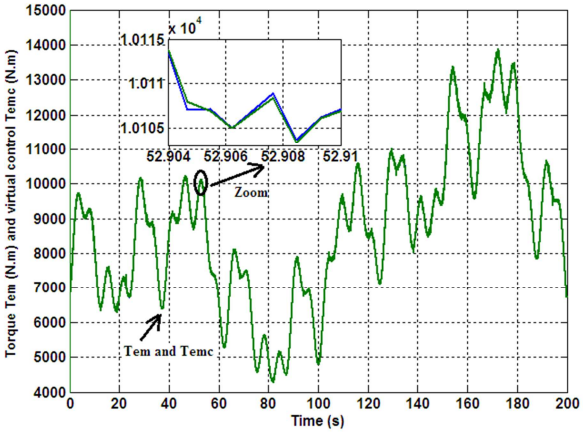

Figure. 3f: Electromagnetic torque and its reference

Journal of Theoretical and Applied Information Technology
10th May 2016. Vol.87. No.1

ISSN: 1992-8645 www.jatit.org E-ISSN: 1817-3195

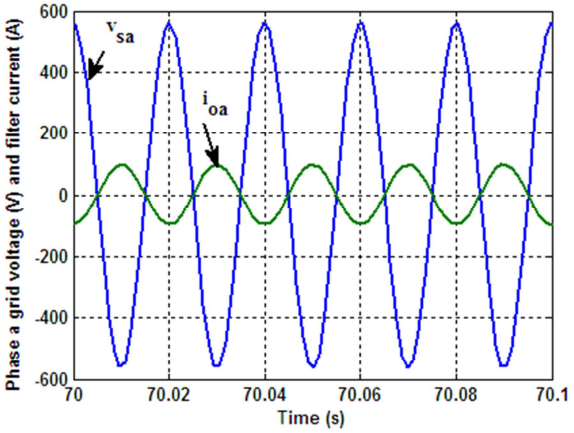

Figure. 3g: Phase a grid voltage and filter current (sub-synchronous speed operation)

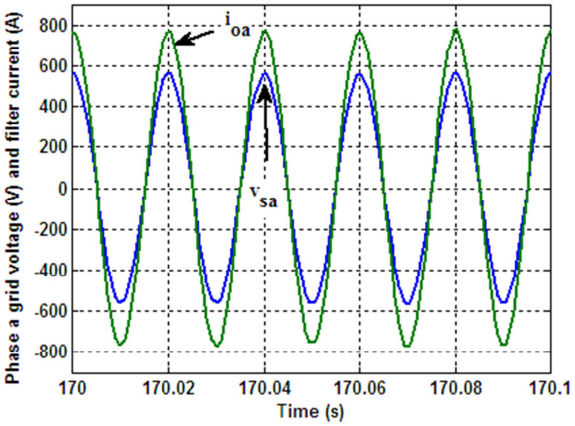

Figure. 3h: Phase a grid voltage and filter current (super-synchronous speed operation)

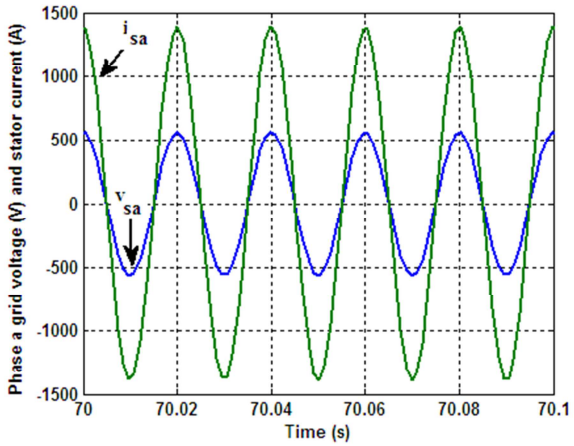

Figure. 3i: Phase a grid voltage and stator current (Sub-synchronous speed operation)

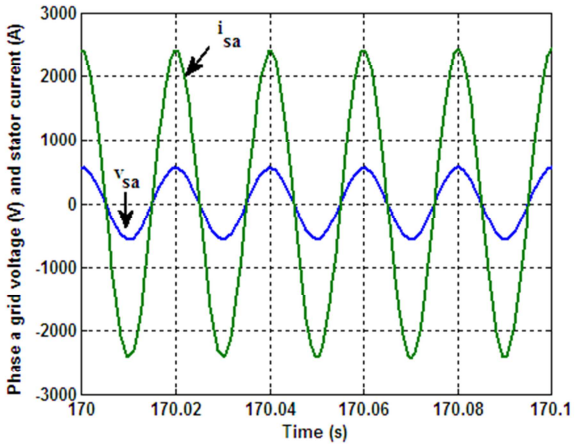

Figure. 3j: Phase a grid voltage and stator current (Super-synchronous speed operation)

Figure 3: Tracking capability under time-varying wind speed

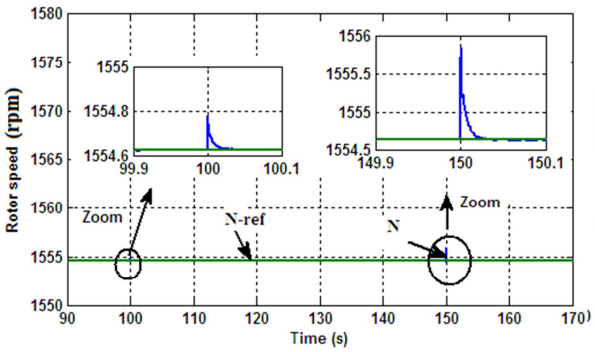

Figure. 4a: Rotor speed with adaptation

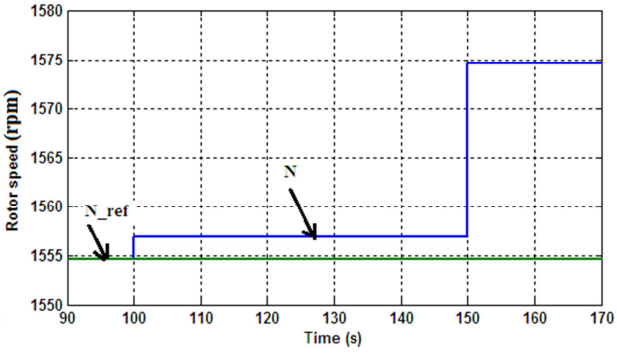

Figure. 4b: Rotor speed without adaptation

Figure 4: Speed Regulation Performance Under Unknown Mechanical Parameters